Journal of Materials and Applications 2025;14(1):1-13
https://doi.org/10.32732/jma.2025.14.1.1

Highly Sensitive and Selective PANI/Ag Nanocomposites-Based Gas Sensors for Room-Temperature NH_3 Detection

Sana Gul Khattak[1], Muhammad Asim Safi[2*], Mutabar Shah[2], Aqib Aziz[2], Yaseen Muhammad[2], Hoor Hassan[2], Humaira Seema[3]

1. Department of Physics, University of Salento, 73100, Italy
2. Department of Physics, University of Peshawar, 25120, Pakistan
3. Institute of Chemical Sciences, University of Peshawar, 25120, Pakistan
E-mail: asimsafi.scientist@gmail.com (Corresponding author)

Received: 14 March 2025; Accepted: 15 April 2025; Available online: 15 May 2025

Abstract: Highly sensitive gas sensors for detection of hazardous gases at room temperature is a critical research area. This study presents the fabrication of NH_3 gas sensors based on polyaniline (PANI) and Polyaniline/silver nanocomposites (PANI/Ag NCs). PANI and Ag NPs were prepared by chemical oxidation and polyol methods, while PANI/Ag NCs were prepared using an ultrasonic-assisted method. XRD analysis confirmed the crystallinity of Ag NPs and the amorphous nature of PANI. SEM images revealed the porous structure of PANI and the uniform distribution of Ag NPs within the PANI matrix. UV–Vis analysis displayed the characteristic absorbance peaks and FTIR analysis confirmed the purity of the synthesized materials. The PANI/Ag (80/20) NC sensor notably displayed significantly improved gas-sensing properties over pristine PANI in terms of higher capacitive and resistive responses, superior sensitivity up to 1047.2%, and faster response/recovery times of 20/6 sec at 36 ppm. The enhanced performance would be ascribed to the enhanced surface area with the incorporation of AgNPs and better electron mobility. The results suggest that PANI/Ag NC-based sensors have excellent potential for efficient room-temperature gas detection.
Keywords: Polyaniline; Silver nanoparticles; Polyaniline/silver nanocomposites; Gas sensors.

1. Introduction

Ammonia (NH_3) is an extremely toxic and corrosive gas used in several contemporary industries, such as agriculture, food processing, and medical services [1, 2]. Nevertheless, minor NH_3 exposure can cause severe health and environmental problems. For this reason, there is an urgent demand for highly sensitive and low-cost gas sensors with the ability to detect all types of dangerous gases at various concentrations from different sources [3]. Polyaniline (PANI), an intrinsically conductive polymer characterized by remarkable electronic conductivity, electrochemical properties, and stability, is an important material for gas sensing applications. The sensitivity of PANI is based on its improved conductivity by charge carrier delocalization within the polymer structure, providing broad ranges for sensing gases such as oxidizing and reducing agents even with very low concentrations in parts per million range [4]. One of the key advantages of PANI is that the reversible process of doping and dedoping with protonic acids, like hydrochloric acid (HCl), significantly improves sensitivity and selectivity towards gases like NH_3 and thereby propels gas sensors for advanced applications [5].

Despite their promise, pristine PANI-based gas sensors often suffer from a slow response time, instability, and limited sensitivity, which severely limits their practical usefulness [6]. Highly ordered structure, solvent selection, unoptimized solution concentration, and evaporation conditions dictate the performance of pristine PANI-based gas sensors [7]. To overcome these difficulties, researchers have tried to introduce metal-metal oxides such as copper (Cu), silver (Ag), zinc oxide (ZnO), tungsten oxide (WO_3), and others into the matrix of PANI to improve the gas-sensing properties [8-11]. For instance, the Cu-doped PANI nanocomposite films prepared by Verma. A. et al. [12] showed outstanding NH_3 gas sensing features with a 51% response at 100 ppm when using PANI@Cu1 and as high as 62% response at 300 ppm when using PANI@Cu5 that had 2 g of Cu nanoparticles, with a recovery time of less than 20 sec. This enhanced performance was credited to doping effect of copper, which altered the electrical properties of PANI, increased interchain separation upon gas interaction, and gave an enormous surface area for gases toward interaction, leading to increased selectivity and sensitivity towards NH_3 compared with other gases. In another study, Rahim, M. et al. [13] synthesized PANI/Bi-ZnO composite sensor which displayed high sensitivity for NH_3 detection, achieving a 20 ppm detection limit and fast response-recovery times of 11-15 sec.

The conductive properties of polyaniline combined with the increased interaction of bismuth-doped zinc oxide with NH_3, resulted in a large change in resistance on exposure to NH_3. Verma, A. et al. [14] explored the potential of sensing NH_3 by the PANI@Ag nanocomposite films. The developed sensor had a gas sensing response of 77% for 100 ppm NH_3 with a recovery time of less than 17 sec. Additionally, it demonstrated selectivity towards NH_3 from other gases. The results were attributed to the efficient adsorption of NH_3 on the surface of the PANI@Ag composite, changing its conductivity, which facilitated the detection process. Based on the work of Aliha, H. M. et al. [15] established that the SnO_2/8 wt% PANI nanocomposite showed improved sensitivity about 187% towards 100 ppm NH_3. The increased depletion barrier height observed for the n-type SnO_2 and p-type PANI p-n heterojunction led to significant resistance drops upon exposure to NH_3 due to charge transfer mechanisms. In addition, increasing the surface area and achieving an optimal distribution of PANI within the composite further improved the rate of adsorption sites created on the ammonia molecules, thus improving sensing capability in general.

Despite these advancements, there are some critical challenges surrounding the scalability of PANI/metal-metal oxide gas sensors. One major issue is achieving high sensitivity and selectivity for target gases, as many PANI/metal sensors struggle with low signal responses and overlapping detection profiles for similar compounds [16]. Complexities in optimized matrix-to-additives ratios for improved chemical response and mechanical robustness remains a significant hurdle [17]. Lastly, the stability and repeatability of these sensors remain a concern, as they may degrade over time or under varying operational conditions [6].

To address these challenges, the current research work is focused on a highly sensitive and selective NH_3 gas sensors using PANI and two novel compositions of polyaniline/silver nanocomposites (PANI/Ag NCs) for achieving high sensitivity, fast response/recovery time, and excellent long-term stability. As-prepared samples were tested for gas sensing behavior within a custom-built gas chamber at room temperature by exposing them to varied NH_3 and methanol (CH_3OH) content. The capacitive and resistive responses toward varying gas content were evaluated and analyzed. The proposed gas sensors showed excellent sensitivity, rapid response/recovery time with long term stability and selectivity towards varying gas content. It can be established that the PANI/Ag NCs have the potential to serve as an appropriate material for gas sensing.

2. Experiemental details

2.1 Materials and chemicals

Silver nitrate ($AgNO_3$), Ethylene glycol (EG), Poly (vinyl pyrrolidone) (PVP-MW- 1,300,000), and ammonium peroxydisulfate $(NH_4)_2S_2O_2$ were obtained from Sigma Aldrich Korea. Aniline hydrochloride ($C_6H_5NH_2$.HCl) and ammonium persulphate (APS) were supplied by Henan Kanbei Chemical Co., Ltd, China and Malaysia Chemical Supplies, respectively. Hydrochloric acid (HCl), acetone, ethanol and dimethylformamide (DMF) were all acquired from Across Organics.

2.2 Synthesis of polyaniline

PANI was synthesized using the chemical oxidative polymerization method [18]. First, 2.59g $C_6H_5NH_2$-HCl was dissolved in 50 mL distilled water. In a separate beaker, 5.71g $(NH_4)_2S_2O_2$ was dissolved in 50 mL distilled water. Both the solutions were then mixed up in a beaker in an acidic medium of HCL and stirred up properly. The acidic nature of the reaction protonated the aniline making it more electrophilic whereas, $(NH_4)_2S_2O_2$, functioning as the oxidizing agent started the polymerization reaction by forming free radicals allowing the coupling of aniline molecules leading to oligomers. The resulting solution was further left at room temperature (RT) for 1 hour showing a clear change in colour from colorless (leucoemeraldine form) to dark green (conductive emeraldine form) of PANI. The color change resulted from the oxidation and protonation process that occurred as aniline monomers were polymerized and polymer chains developing a conjugated structure, indicating the successful formation of PANI. The final product was obtained by washing it with 100 mL HCL and acetone to remove all impurities, and then was dried vacuum.

2.3 Synthesis of silver nanoparticles

Polyol method was utilized to synthesize the Ag nanoparticles (NPs) [19]. Initially, $AgNO_3$ and PVP were prepared by dissolving appropriate amounts of PVP and $AgNO_3$ in ethylene glycol (EG) in separate beakers under constant magnetic stirring at RT. Subsequently, 2 mL of EG was heated to 120 °C for about 10 min. After that, 0.00003 g of $AgNO_3$ was directly added to 1 mL of EG. After 15 min, a solution of 0.005 g $AgNO_3$ dissolved in 5 mL of EG was injected to the reaction system using a syringe. This was followed by the injection of 0.333 g of PVP dissolved in 10 mL of EG, which was added over a 10-minute period. The reaction mixture was kept at 110 °C under continuous stirring for 2 hours. Change of color solution from bright yellow to gray during this period indicated successful nucleation and growth of Ag NPs. The product was diluted using acetone, then centrifuged at 4000 rpm for 25 min, allowing the Ag NPs to settle down at the bottom of the centrifuge tube. This was followed

by the careful removal of EG suspension via pipette. Ethanol was added to the tube to disperse NPs and dissolve any residual PVP. Post second centrifugation, the cleansed Ag NPs were kept in ethanol for subsequent characterization.

2.4 Synthesis of polyaniline/silver nanocomposites

The synthesis of the PANI/Ag NCs was performed using an ultrasonic-assisted solution process. First, 0.05 g of Ag NPs and 0.05 g of PANI were separately dispersed in 1 mL of dimethylformamide (DMF) and sonicated for 45 min to obtain a clear, uniform solution. In the next step, two novel compositions of PANI/Ag NCs were prepared. First, 0.005 g of Ag and 0.045 g of PANI were mixed in 1 mL of DMF solvent and sonicated for 1 hr. This resulted in a uniform NC solution of PANI/Ag NC that was termed PANI/Ag (90/10) NC. The same procedure was repeated for NC compositions, titled PANI/Ag (80/20) NC, by mixing 0.01 g of Ag and 0.04 g of PANI in 1 mL of DMF solvent.

2.5 Materials characterization and sensor fabrication

Specimens were investigated for their microstructural properties by a diffractometer X-ray (JDX-3532, JEOL, Japan) over a 2θ-range of 20°-80°, whereas scanning electron microscope (JSM 5910, JEOL, Japan) was used to examine the surface morphology. Additionally, optical properties were measured in a wavelength range of 200-800 nm using a Shimadzu UV–VIS-NIR double-beam spectrophotometer (SolidSpec-3700). A Fourier Transform Infrared Spectrometer, from Shimadzu Scientific Instruments, was utilized to measure the existence of various functional groups and chemical bonds in the prepared materials between 450 and 4000 cm^{-1}.

For the investigation of gas sensing properties, the synthesized PANI and PANI/Ag NCs were spin coated onto the interdigitated electrodes (IDEs) surface and positioned within a custom build gas chamber. The fabricated sensors were subjected to various concentration of NH_3 and CH_3OH and the electrical properties were evaluated at different testing frequencies (100 Hz-2 kHz) using GW INSTEK 817 LCR meter. The schematics of PANI, Ag synthesis and sensor's assembly are displayed in Fig. 1(a-c).

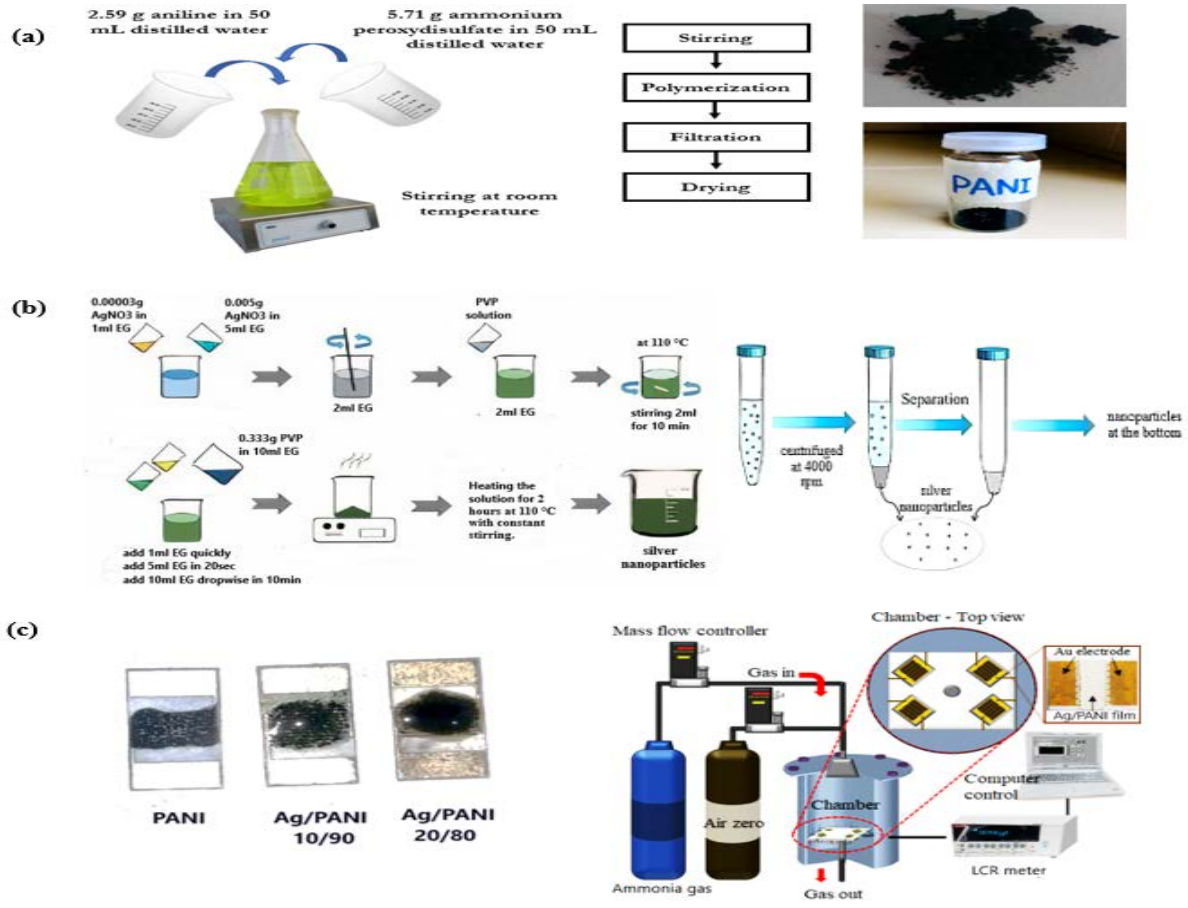

Fig.1. (a) Schematic flow chart of chemical oxidative polymerization for the synthesis of PANI. (b) Schematic flow chart of Silver NPs obtained via polyol method. (c) Fabricated sensors and Gas sensing setup.

3. Results and discussion

3.1 Uv–vis absorption spectroscopy analysis

Fig. 2(a) displays the absorption spectra of the synthesized samples with PANI, showing an absorption peak at 361 nm corresponding to π-π* transition of the benzenoid ring. This resulting from its conjugated structure that allows for the delocalization of π electrons across the polymer chain [20]. Ag NPs exhibited a pointed peak at 433 nm corresponding to surface plasmon resonance [21]. The spectra of PANI/Ag (90/10) and PANI/Ag (80/20) NC revealed absorbance peaks at 379 nm and 371 nm, respectively, that was shifted towards the blue region as compared to the Ag spectrum. The occurrence of blue shift is ascribed to the Ag NPs facilitating the electron transfer between Ag and the π-conjugated system of PANI, altering the polymer's electronic structure and shifting the π-π* transitions. Additionally, higher concentration of Ag NPs dopants in PANI/Ag (80/20) NC modified the protonation states and doping level of PANI, resulting in a decreased conjugation length and further shifting the absorbance to a shorter wavelength [12].

The optical band gap for PANI, Ag NPs and PANI/Ag NC as displayed in Fig. 2(b) were calculated by the Tauc equation [22]. The direct bandgap of Ag NPs was calculated to 3.55 eV while that of PANI was 4.07 eV. The indirect band gap of PANI/Ag NC was estimated to be 2.28 eV. The significant reduction in the optical bandgap of the PANI/Ag NC compared to pristine PANI and Ag NPs can be attributed to charge transfer between the two materials, plasmonic effects from Ag nanoparticles, and strong interfacial interactions. These factors lead to the formation of new electronic states, a shift in the Fermi level, and enhanced light absorption, all of which contribute to the decrease in the bandgap [23].

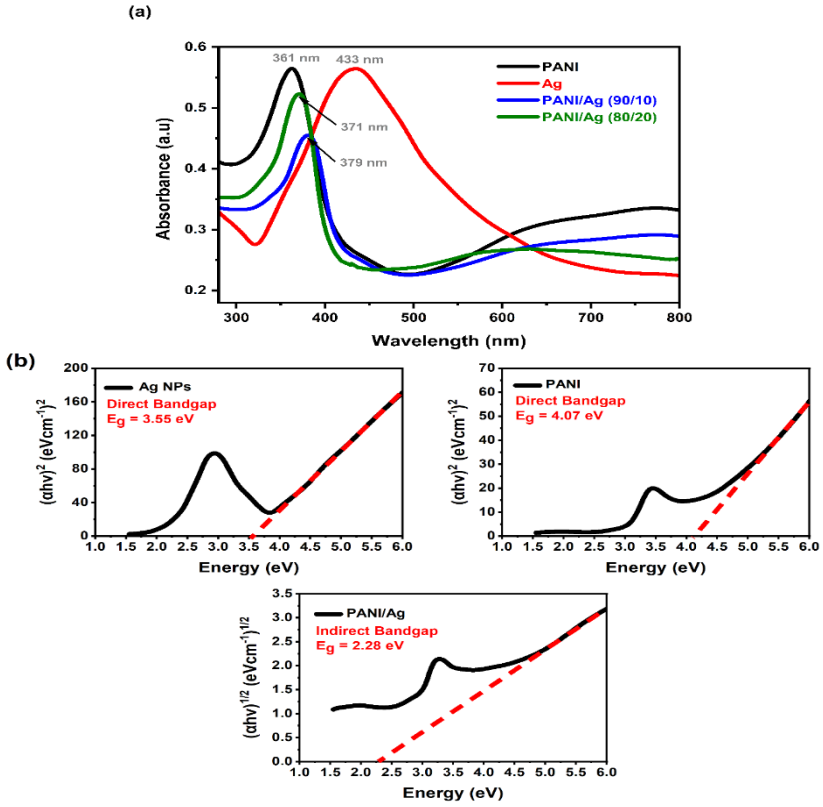

Fig. 2. (a) Absorbance spectra of PANI, Ag NPs, PANI/Ag (90/10) NC and PANI/Ag (80/20) NC and (b) Optical bandgaps of PANI, Ag NPs, PANI/Ag NC.

3.2 Fourier transform infrared spectroscopy analysis

Fig. 3 shows the FTIR spectra of synthesized materials. Ag NPs FTIR spectrum shows absorption peaks at 3412 cm^{-1} and 2950 cm^{-1} ascribed to the -OH stretching. The peak at 1685 cm^{-1} was attributed to the C=O extending arising from the carboxyl group. The 1402 cm^{-1} and 1063 cm^{-1} absorbance peaks are ascribed to the CO-NH and C-N vibrations from the amide-associated groups [24]. In the FTIR spectrum of PANI, a strong peak at 3733 cm^{-1} appears owing to the N-H stretching of the PANI amino group. The peak at 3430 cm^{-1} appears due to -OH stretching. The peak at 2336 cm^{-1} is due to the n(N-H) plus unsaturated amine group. The peak around 1562 cm^{-1}

is assigned as due to the C=C stretching, while the peak at 1063 cm^{-1} is attributed to the B-NH-B group from the benzenoid ring [25]. All the major bands of PANI/Ag NCs are present in the spectra of PANI. The FTIR spectra of PANI/Ag NCs are showing the interaction of Ag NPs with different reaction sites of PANI with slightly decreased intensities of peaks of PANI. The mode at 1330 cm^{-1} has been assigned to the stretching of C-N that is in the secondary amine. And the band at 1072 cm^{-1} is attributed to the in-plane bending.

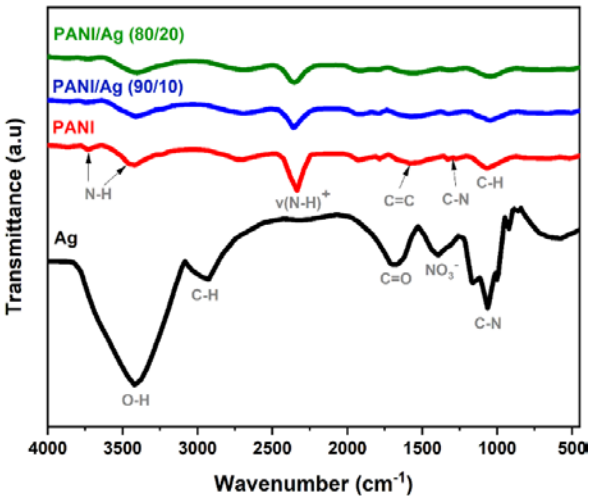

Fig. 3. FTIR spectra of PANI, Ag NPs, PANI/Ag (90/10) NC and PANI/Ag (80/20) NC.

3.3 Microstructural and phase analysis

Fig. 4(a-e) presents the XRD spectra of the synthesized specimens. The XRD spectra of Ag NPs reveals a face-centered cubic (FCC) crystal structure, characteristic of metallic silver [26]. The diffractogram, as depicted in Fig. 4(a) exhibits well-defined Bragg reflections at 2θ values of 38.12°, 44.16°, 64.35°, and 77.34°. These peaks correspond to the (111), (020), (022), and (131) crystallographic planes, respectively, with associated interplanar d-spacings of 2.358 Å, 2.048 Å, 1.446 Å, and 1.233 Å. The observed diffraction pattern aligns precisely with the Crystallography Open Database (COD) Card Number 96-110-0137 for Ag, confirming phase purity of the synthesized NPs. The absence of extraneous peaks indicates the establishment of single-phase, highly crystalline Ag NPs without detectable impurities or secondary phases [26]. The sharp and intense nature of the diffraction peaks suggests a high degree of crystallinity and long-range order within the Ag NPs. Lattice parameter refinement yields values of a = b = c = 4.094 Å for the Ag NPs, which is in close agreement with both the COD Reference Card values and previously reported literature (a = b = c = 4.0887 Å), affirming the phase identity as cubic Ag (Fm-3m, space group number 225) [26]. The prominent reflection corresponding to the (111) plane at 38.12° indicates preferential orientation in the cubic phase. This orientation is typical of nanoscale Ag, where the (111) facet is thermodynamically stable due to its low surface energy [26]. Table 1 provides a relative analysis of the lattice constants for the synthesized Ag NPs against COD Reference Card values and previous studies. The XRD pattern of PANI shows a single broad diffraction peak at 2θ = 25.12°, credited to the (200) plane with d-spacing = 3.5450 Å. The presence of a single broad peak and absence of other weak peaks indicates the amorphous nature of PANI. This is consistent with the typical structure of PANI, which often exhibits low crystallinity [27]. The XRD patterns for PANI/Ag NCs show similarities to the Ag NPs pattern but with reduced peak intensities. The decreased intensity correlates with increasing Ag content, suggesting a possible interaction between PANI and Ag nanoparticles.

The Debye Sherrer equation was used to calculate the crystalline size of Ag NPs [28]:

$$D = k\lambda/\beta\cos\theta \quad (1)$$

The crystallite size calculations of Ag NPs yielded an average value of 18.56 nm, with individual values ranging from 15.62 nm to 22.97 nm for different crystallographic planes. This range indicates a degree of anisotropy in crystallite growth. The (111) plane exhibited the largest crystallite size of 22.97 nm, suggesting preferential growth along this direction. The obtained crystallite sizes are consistent with those reported by Zaman, Y. et al [28], indicating reproducibility in the synthesis method. The nanoscale dimensions of the crystallites contribute to the unique properties of Ag NPs, such as enhanced surface area-to-volume ratio [29]. Table 2 presents the summary of diffraction angle (2θ), Full Width Half Maximum (FWHM), and calculated values of crystallite size (D_{hkl}) of Ag NPs.

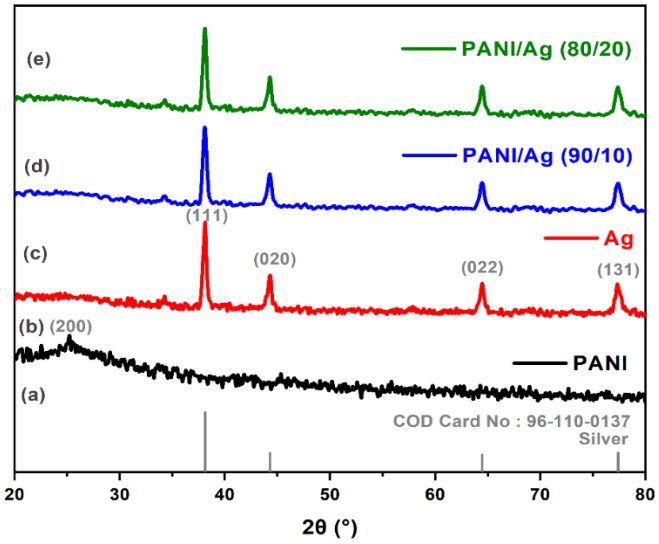

Fig. 4. XRD patterns of (a) COD Card No for Ag, (b) PANI, (c) Ag NPs, (d) PANI/Ag (90/10) NC, and (e) PANI/Ag (80/20) NC.

Table 1. Relative analysis of the lattice constants of Ag NPs.

Material	Lattice Parameters
Ag NPs	**a = b = c**
COD Card Values	4.086
Al-Mahmud, M. R. et al. [27]	4.087
This Work	4.094

Table 2. Summary of a diffraction angle (2θ), Full Width Half Maximum (FWHM), and calculated values of crystallite size (D_{hkl}) of Ag NPs.

Material	Diffraction angle (2θ)	Full Width Half Maximum (FWHM)	Crystallite Size (nm)	Average Crystallite Size (nm)
Ag NPs	38.12°	0.384	22.97	**18.56**
	44.16°	0.576	15.62	
	64.35°	0.576	17.10	
	77.34°	0.576	18.54	

3.4 Surface morphology analysis

Fig. 5(a-d) presents the SEM micrographs of the synthesized Ag NPs, PANI, and PANI/Ag NCs at X10,000 magnification and 1µm scale bar, providing insight into their surface morphology. Fig. 5(a) shows the SEM image of PANI, which demonstrates a porous and amorphous morphology. The interconnected porous network observed in PANI allows for facile diffusion of external gas molecules, contributing to enhanced charge transport and surface interaction properties. The porosity of the PANI matrix facilitates its potential use in sensing and catalytic applications by providing a large surface area for adsorption [30]. Fig. 5(a) shows the fairly uniform dispersion of the quasi-spherical Ag NPs. Surface-voids and pores present on the Ag NPs suggest their potential for enhanced gas adsorption, which has potentials in gas-sensing applications. These features reflecting high surface-to-volume ratio, are essential for the enhancement of both electrical conductivity and sensitivity [31]. In Fig. 5(c) and 5(d), the Ag NPs are well incorporated into the PANI matrix, with NCs displaying an even dispersion of Ag NPs on the PANI surface. The successful integration of Ag NPs within the hollow areas of the PANI structure resulted in an evidently smoother and compact surface. High surface-to-volume ratio of the Ag NPs had made them merge into the PANI matrix and had formed agglomerated NC structures. Nonetheless, some parts of the micrograph reflect less agglomeration, likely due to the high surface energy of Ag NPs. This suggest that the PANI matrix effectively stabilized the Ag NPs and mitigated excessive particle coalescence. This heterogeneous distribution may be resulted from localized variations in the NP concentration or differences in the polymer-nanoparticle interactions across the sample [32].

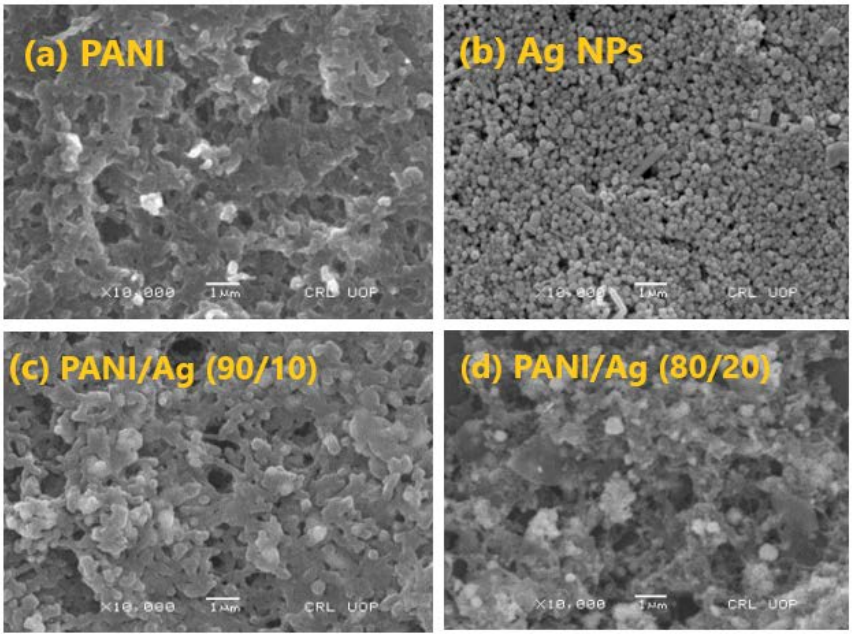

Fig. 5. SEM images of (a) PANI, (b) Ag NPs, (c) PANI/Ag (90/10) NC, and (d) PANI/Ag (80/20) NC at X10,000 magnification and 1µm scale bar.

3.5 Gas sensing characteristics

The fabricated PANI and PANI/Ag NC-based sensors were systematically inspected for their gas sensing performance through the measurement of electrical responses to different NH_3 concentrations ranging from 2.6 ppm to 36 ppm at operational frequencies of 100 Hz, 500 Hz, 1 kHz, and 2 kHz. Fig. 6(a) displays the capacitance variation of the sensors as a function of NH_3 concentration, measured at different applied frequencies. The sensors demonstrated a direct correlation between the NH_3 concentration and the measured capacitance, with PANI/Ag NC-based sensors exhibiting superior capacitance compared to pristine PANI-based sensor across the tested NH_3 concentration range. The PANI/Ag (90/10) NC-based sensor exhibited a maximum capacitance of 198.842 pF, while the PANI/Ag (80/20) NC-based sensor reached 569.474 pF upon exposure to 36 ppm NH_3 at 100 Hz. In contrast, the pristine PANI sensor displayed a comparatively lower capacitance of 92.542 pF under identical conditions.

The increase in capacitance due to NH_3 exposure can be attributed to the interaction of NH_3 molecules with the oxygen species adsorbed on the surface of the sensor. Upon absorption, a redox reaction occurs between these oxygen species and NH_3, leading to the release of electrons into the conduction band of the sensor material. The process increases electron charge carriers on the active material surface, making the polarization of the dielectric stronger and increases the capacitance [33]. In the case of PANI/Ag NC, the high surface area and catalytic nature of the Ag NPs introduced more active adsorption sites. This further increased electron transfer when exposed to NH3. As a result, the capacitive response of PANI/Ag NCs is significantly higher as compared to pristine PANI [33]. Furthermore, the frequency-capacitance plot displayed a reverse trend, and capacitance decreased with an increase in frequency. This could be related to a polarizability dependent on frequency of the sensing material. The dipoles in the material will have no adequate time to align with the alternating electric field at high frequency levels; polarization falls, and consequently, capacitance values are also less [33].

The fabricated PANI and PANI/Ag NC-based gas sensors also displayed excellent resistive characteristics as depicted in Fig. 6(b). The sensors exhibited a significant decrease in resistance with increasing NH_3 concentration, demonstrating their excellent sensitivity to NH_3. Pristine PANI sensor displayed a substantial resistance reduction from 494.56 KΩ to 120.64 KΩ, corresponding to a 75.60% decrease. Similarly, the PANI/Ag (90/10) NC sensor showed a reduction in resistance from 431.33 KΩ to 123.41 KΩ (71.38% decrease), while the PANI/Ag (80/20) NC sensor exhibited the most pronounced response, with its resistance decreasing from 380.08 KΩ to 71.77 KΩ, an 81.11% reduction, at 100 Hz.

The underlying mechanism responsible for this decrease in resistance can be attributed to the interaction of NH_3 molecules with the sensor's active material, which enhances the material's conductivity. NH_3, being an electron-donating gas, undergoes adsorption on the sensor surface, where it interacts with protonated sites on the PANI and PANI/Ag NC matrix. The deprotonation of these sites upon NH_3 adsorption results in an increase in the number of free electrons in the conduction band, effectively increasing the sensor's overall conductivity and consequently

an observed decrease in resistance [34]. The enhanced performance of the PANI/Ag (80/20) NC sensor, which shows the largest resistance decrease, can be explained by the increased concentration of Ag NPs within the NC. A higher concentration of Ag NPs leads to a greater density of conductive channels and adsorption sites, allowing for a more significant interaction between NH_3 molecules and the sensing material. This results in a more pronounced reduction in resistance, as reflected by the graph data [34].

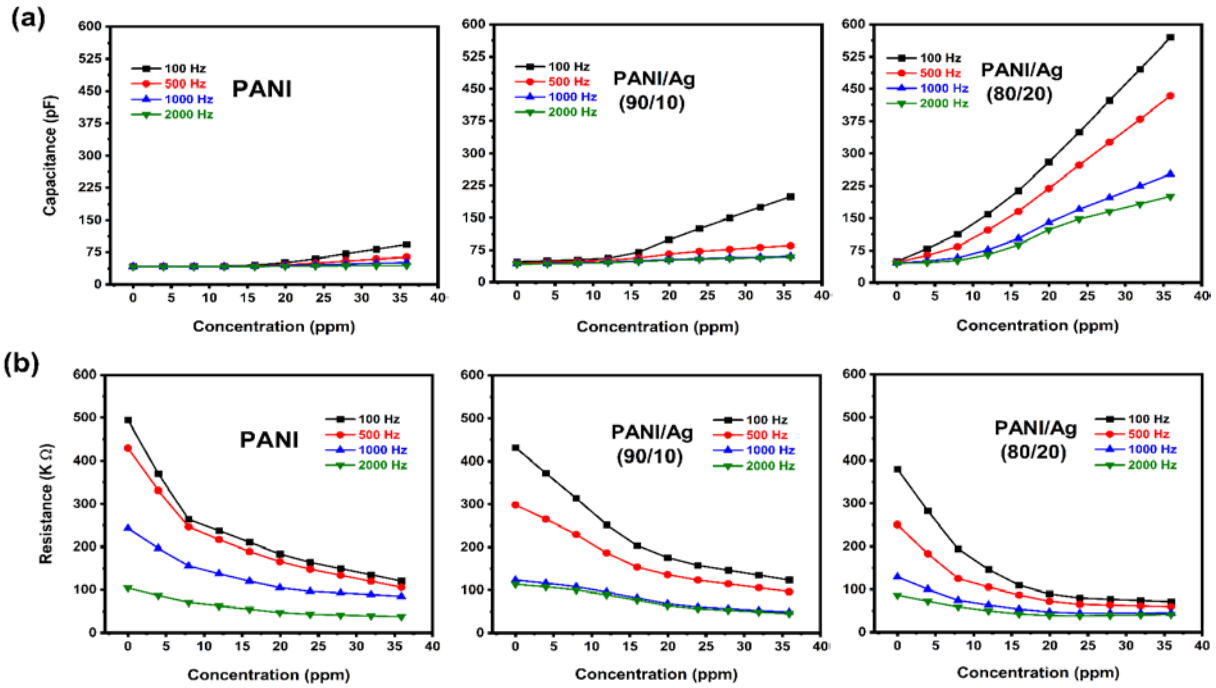

Fig. 6. (a) Variation in capacitance, and (b) Variation in resistance of PANI, PANI/Ag (90/10) NC, and PANI/Ag (80/20) NC towards increasing NH_3 at diverse frequencies.

One of the critical criteria for determining the performance of a gas sensor is sensitivity, which provides an estimate of their capability to detect different concentrations of a gas under various conditions. Capacitive sensitivity *S%* for the developed sensor was determined as follows:

$$S\% = (C_g - C_o)/C_o \times 100 \quad (2)$$

where C_g is the capacitance of the sensor when NH_3 gas has been introduced, and C_o the capacitance in air. Fig. 7(a) shows how the capacitive sensitivity evolved across varying frequencies and NH_3 concentrations. The results showed that with an increase in NH_3 concentration, the capacitive sensitivity increased for all sensor types tested. This improvement is ascribed to the enhanced adsorption of NH_3 molecules on the active surface of the sensor, which further boosted electron transfer between the NH_3 molecules and the sensor material, hence improving its response to changes in gas concentration [33]. The highest capacitive sensitivity, 1047.2% at 100 Hz, was observed for the PANI/Ag (80/20) NC sensor; the sensitivity values for the sensors based on the PANI/Ag (90/10) NC and pure PANI were 317.7% and 116.7%, respectively. The superior performance of the PANI/Ag (80/20) NC sensor can be attributed to its larger surface area and improved conductivity, thanks to the higher concentration of Ag NPs. Ag NPs acted as electron reservoirs that supported the charge transfer during the NH_3 adsorption process. The growth of surface charge carriers onto the sensor surface significantly enhanced the capacitive response. The more NH_3 molecules adsorbed onto the sensor, the greater the polarization effects occurring in the sensor material and thus increased capacitive sensitivity [33]. In addition, the capacitive sensitivity was inversely proportional to the increase in frequency, aligning with typical behavior of the dipole polarization mechanism [33].

Resistive sensitivity of the sensors was also determined by calculating the percentage change in resistivity using the following formula:

$$S\% = (R_o - R_g)/R_g \times 100 \quad (3)$$

where R_o is the resistance of sensor in air, and R_g is the resistance when exposed to NH_3 gas. Fig. 7(b) shows the variation of resistive sensitivity across different frequencies and NH_3 concentrations. Resistive sensitivity increased with higher NH_3 concentrations for all the sensor types. The maximum resistive sensitivity was achieved by the sensor based on PANI/Ag (80/20) NCs, which reached 81.11% at 36 ppm of NH_3 at 100 Hz. Resistive sensitivities of the PANI sensor and the PANI/Ag (90/10) NC sensor under similar conditions were 75.60% and 71.38%, respectively. The rise in resistive sensitivity can be linked to NH_3 molecules interaction with the sensor material, effecting its electrical conductivity [35]. Ag NPs in the PANI/Ag NC-based sensors played an important role in enhancing the resistive sensitivity. Due to their high conductivity and surface energy, Ag NPs provided more active sites for NH_3 adsorption, enabling faster charge transfer. The higher concentration of Ag NPs in the PANI/Ag (80/20) NC sensor offered more adsorption sites, strengthening the interaction between NH_3 molecules and the surface of the sensor. This resulted in a larger resistance reduction and, consequently, the greater resistive sensitivity [34].

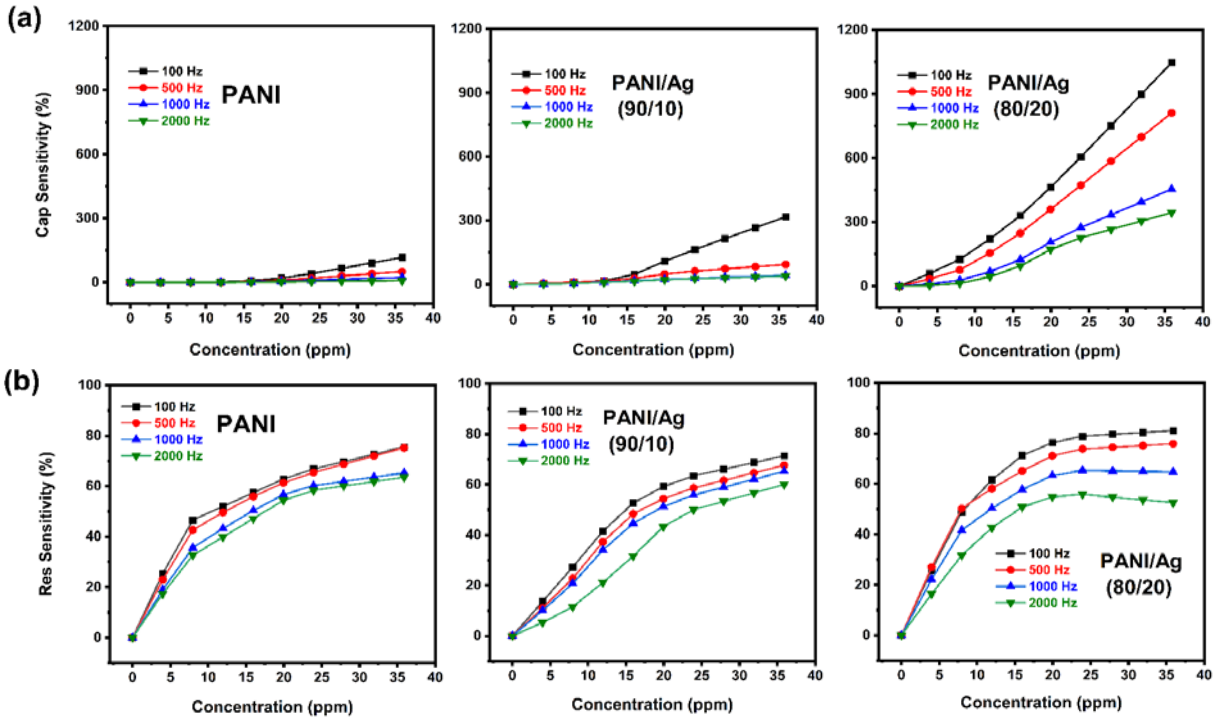

Fig. 7. (a) Capacitive sensitivity, and (b) Resistive sensitivity of PANI, PANI/Ag (90/10) NC, and PANI/Ag (80/20) NC towards varying NH_3 at different frequencies.

Stability is a very important parameter for assessing the long-term performance and reproducibility of a gas sensor. Herein, the stability of PANI and PANI/Ag NC-based fabricated gas sensors has been particularly assessed by observing their capacitive response towards 7 ppm, 21 ppm, and 36 ppm concentrations of NH_3 over a period of 30 days. Results as illustrated in Fig. 8, shows that the sensors displayed outstanding stability throughout the test period, exhibiting less than a 3% variation in capacitance across all tested NH_3 concentrations. Superior stability in the sensors can be mainly attributed to the structural robustness of the PANI matrix and the reinforcing effect of Ag NPs in the PANI/Ag NC-based sensors [14].

The response and recovery times are another important parameter for assessing the gas sensor performance. In this study, the response/recovery curves of gas sensors were evaluated by exposing the sensors to 7 ppm, 21 ppm, and 36 ppm NH_3 at different frequencies. It was seen that as the NH_3 concentration increased, both the response and recovery times decreased considerably. This can be credited to the fact that at higher concentration NH_3 molecules were adsorbed more quickly onto the sensor surface, which allowed faster electron transfer and quicker establishment of capacitive equilibrium. The increasing gas concentration improved the diffusion of NH_3 molecules into the porous sensing layer, consequently accelerating the gas-sensing process and the resulting capacitive response. Thus, the active sensing material reaching its saturation much faster. At higher concentrations, the reduced recovery time most probably resulted from the immediate desorption of gas molecules from the sensor's surface. Once the NH_3 concentration increased, surface coverage by the sensing material expanded, leading to faster electron return to the conduction band during the desorption phase. This mechanism ensured a more rapid restoration of the sensor's baseline capacitance values [33]. Fig. 9 provide a visual representation while

Table 3 represents the summary of the response and recovery times as functions of NH_3 concentration and frequency. Notably, the PANI/Ag (80/20) NC-based gas sensor demonstrated the fastest response/recovery time of 20/6 sec when subjected to 36 ppm NH_3 at 100 Hz. This superior performance is likely due to the synergistic effect of the Ag NPs, which improved electron mobility, and the conductive nature of polyaniline, ensuring rapid charge transfer dynamics during both adsorption and desorption phases [34]. Table 4 shows the comparative study with the previous research works, displaying vast improvement in response and recovery times.

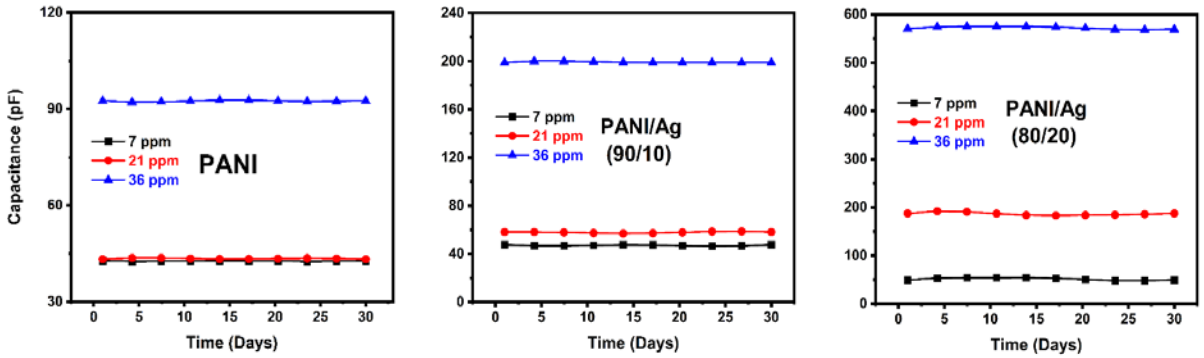

Fig. 8. Variation in capacitance in time of PANI, PANI/Ag (90/10) NC, and PANI/Ag (80/20) NC-based gas sensors.

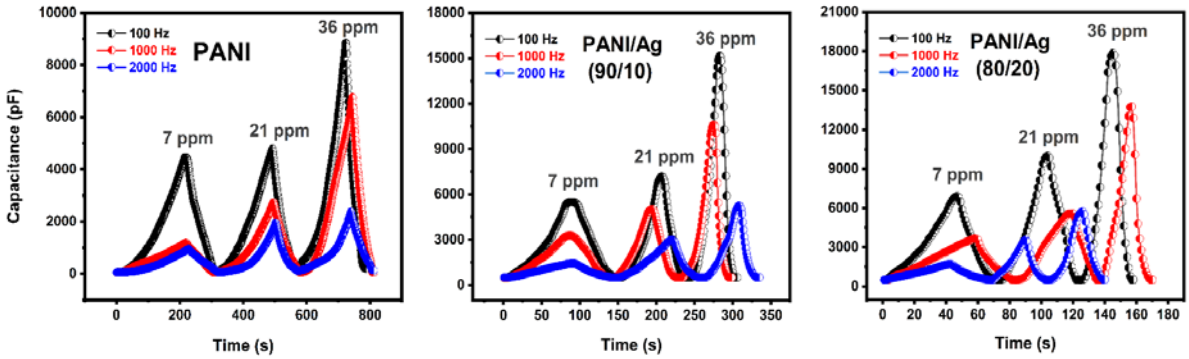

Fig. 9. Response/recovery time of PANI, PANI/Ag (90/10) NC, and PANI/Ag (80/20) NC gas sensors towards varying NH_3 concentration at 100 Hz.

Table 3. Response and recovery time for fabricated sensors at 100 Hz under various NH_3 Concentrations.

Sensing Material	**PANI**	**PANI/Ag (90/10)**	**PANI/Ag (80/20)**
Conc: Freq (100 Hz)	**Res/Rec Time (s)**	**Res/Rec Time (s)**	**Res/Rec Time (s)**
7 ppm	210/105	83/49	49/23
21 ppm	175/80	56/24	27/15
36 ppm	150/67	38/18	20/6

Table 4. Comparative analysis of response and recovery times with the previous research works.

Materials	**Gas**	**Concentration (ppm)**	**Response Time (sec)**	**Recovery Time (sec)**	**Reference**
PANI	NH_3	0.5-10	48	185	[35]
PANI/NiO	NH_3	10	149	257	[36]
PANI/ZnO	NO_2	10	32	50	[37]
PANI/SnO_2	H_2	6000	11	7	[38]
PANI/Ag-decorated ZnO	NH_3	5-120	23	58	[39]
PANI/ln_2O_3	NO_2	0.3-100	17.28	91.26	[40]
PANI/CuO	H_2S	2-25	36	71	[41]
PANI	NH_3	36	150	67	This Work
PANI/Ag (90/10)	NH_3	36	38	18	This Work
PANI/Ag (80/20)	NH_3	36	20	6	This Work

A comparative analysis of the fabricated gas sensors was performed to evaluate their sensing behavior towards NH_3 and CH_3OH gases. As shown in Fig. 10(a-d), the fabricated sensors displayed superior gas sensing characteristics towards NH_3 compared to CH_3OH. This performance disparity is primarily attributed to the stronger electron-donating nature and higher volatility of NH_3 compared to CH_3OH. NH_3, being a potent Lewis base, has a pronounced electron donation ability, which facilitates more efficient interaction with the sensor's active surface, thereby leading to a greater modulation in the sensor's capacitance and resistance. The faster evaporation rate of NH_3 further contributes to the sensor's enhanced response by ensuring rapid diffusion and adsorption of NH_3 molecules on the sensing material [34].

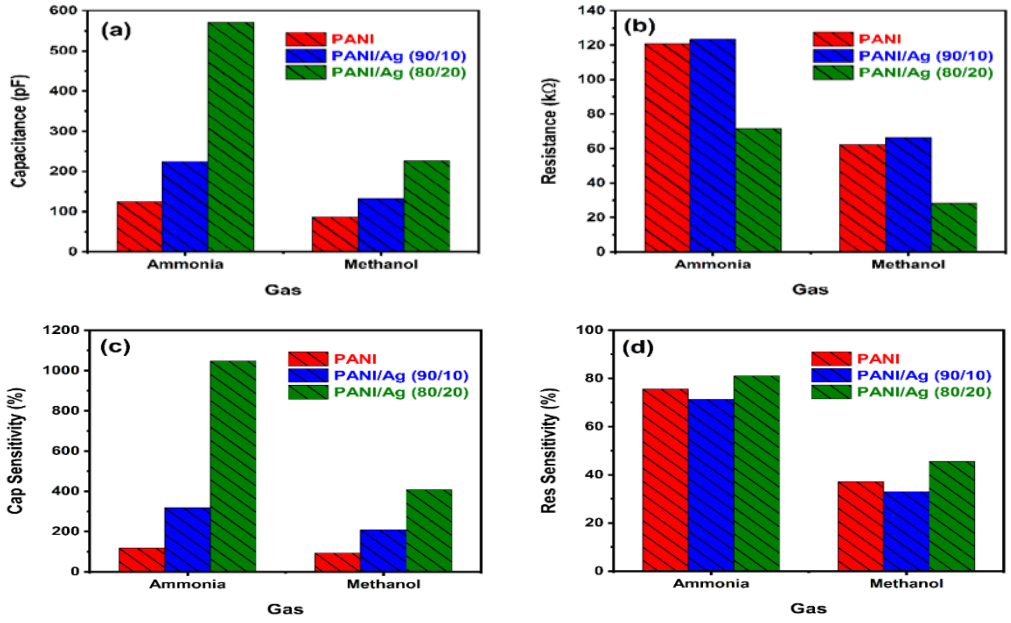

Fig. 10 Comparison of (a) capacitance, (b) resistance, (c) capacitive sensitivity, and (d) resistive sensitivity of PANI, PANI/Ag (90/10) NC, and PANI/Ag (80/20) NC towards NH_3 and CH_3OH.

4. Conclusions

In summary, PANI, and PANI/Ag NCs-based gas sensors were successfully fabricated and analyzed for gas sensing characteristics. PANI and Ag NPs were synthesized via chemical oxidation and polyol method whereas, the PANI/Ag NCs were prepared using the ultra-sonic assisted method. The XRD results confirmed the crystallinity of Ag NPs and amorphous nature of PANI. SEM images showed the porous structure of PANI and uniform dispersal of Ag NPs within the PANI medium. UV–Vis and FTIR analysis confirmed the presence of characteristic absorbance peaks and purity of materials. The experimental results demonstrated that PANI/Ag NCs, particularly PANI/Ag (80/20), exhibited superior gas-sensing performance compared to pristine PANI. The enhanced performance, including higher sensitivity, faster response/recovery times, and stability, was ascribed to the synergistic properties of Ag NPs, which increased the surface area and improved charge transfer. These findings indicate the strong potential of PANI/Ag NCs for efficient NH_3 gas detection at room temperature.

5. Acknowledgments

The authors are thankful to Pakistan Council of Scientific and Industrial Research (PCSIR), Institute of Chemical Sciences and Organic Nano Device Laboratory (ONDL), Department of Physics, University of Peshawar for their valuable support in completion of this research work.

6. References

[1] Saxena P, Shukla P. A review on recent developments and advances in environmental gas sensors to monitor toxic gas pollutants. Environmental Progress & Sustainable Energy. 2023;42(5):e14126.
[2] Chamoli A, Bhambri A, Karn SK, Raj V. Ammonia, nitrite transformations and their fixation by different biological and chemical agents. Chemistry and Ecology. 2024;40(2):166-199.

[3] Lawaniya SD, Kumar S, Yu Y, Rubahn H-G, Mishra YK, Awasthi K. Functional nanomaterials in flexible gas sensors: recent progress and future prospects. Materials Today Chemistry. 2023;29:101428.
[4] Singh A, Dipak P, Iqbal A, Samadhiya A, Dwivedi SK, Tiwari DC, et al. Fast response and recovery polyaniline montmorillonite reduce graphene oxide polymer nanocomposite material for detection of hydrogen cyanide gas. Scientific Reports. 2023;13(1):8074.
[5] Li B, Li Y, Ma P. Synthesis of different inorganic acids doped polyaniline materials and behavior of enhancing NH3 gas sensing properties. Organic Electronics. 2023;114:106749.
[6] Zhu C, Zhou T, Xia H, Zhang T. Flexible room-temperature ammonia gas sensors based on pani-mwcnts/pdms film for breathing analysis and food safety. Nanomaterials. 2023;13(7):1158.
[7] Peykari M, Pourmahdian S. Developing a ternary conductive hydrogel of polyacrylamide, polyaniline, and carbon nanotube: A potential chemiresistive gas sensor. Journal of Composite Materials. 2023;57(27):4291-4305.
[8] Mathankumar G, Harish S, Mohan MK, Bharathi P, Kannan SK, Archana J, Navaneethan M. Enhanced selectivity and ultra-fast detection of NO2 gas sensor via Ag modified WO3 nanostructures for gas sensing applications. Sensors and Actuators B: Chemical. 2023;381:133374.
[9] Adhav P, Pawar D, Diwate B, Bora M, Jagtap S, Chourasia A, et al. Room temperature operable ultra-sensitive ammonia sensor based on polyaniline-silver (PANI-Ag) nanocomposites synthesized by ultra-sonication. Synthetic Metals. 2023;293:117237.
[10] Foronda JRF, Aryaswara LG, Santos GNC, Raghu SN, Muflikhun MA. Broad-class volatile organic compounds (VOCs) detection via polyaniline/zinc oxide (PANI/ZnO) composite materials as gas sensor application. Heliyon. 2023;9(2).
[11] Jaiswal R, Joshi MC, Ramadurai R, Sunkara M, Kannan V, editors. Structural and electrical conductivity studies of Polyaniline-WO3 hybrid nanocomposites for gas sensing applications. Journal of Physics: Conference Series; IOP Publishing. 2024.
[12] Verma A, Kumar T. Gas sensing properties of a Cu-doped PANI nanocomposite towards ammonia. Materials Advances. 2024;5(18):7387-7400.
[13] Rahim M, Ullah R, Ahmad N, Rahim I, Yaseen S. Synthesis and characterization of highly sensitive ammonia sensor based on polyaniline/bismuth doped zinc oxide composites. Polymer Composites. 2024.
[14] Verma A, Kumar T. PANI@ Ag nanocomposites gas sensors for rapid detection of ammonia. Polyhedron. 2024;255:116982.
[15] Aliha HM, Khodadadi AA, Mortazavi Y, Lotfollahi MN. Novel SnO2/PAni nanocomposites for selective detection of ammonia at room temperature. Applied Surface Science. 2023;615:156381.
[16] Faricha A, Yoshida S, Chakraborty P, Okamoto K, Chang T-FM, Sone M, Nakamoto T. Array of miniaturized amperometric gas sensors using atomic gold decorated Pt/PANI electrodes in room temperature ionic liquid films. Sensors. 2023;23(8):4132.
[17] Kaur R, Lawaniya SD, Kumar S, Saini N, Awasthi K. Nanoarchitectonics of polyaniline–zinc oxide (PANI–ZnO) nanocomposite for enhanced room temperature ammonia sensing. Applied Physics A. 2023;129(11):765.
[18] Abbood AS, Ibraheem IJ. Polyaniline Nano Films Synthesis in One Step via Chemical Oxidative Polymerization. Baghdad Science Journal. 2024;21(2):0401.
[19] Ahmad I, Khan MN, Hayat K, Ahmad T, Shams DF, Khan W, et al. Investigating the Antibacterial and Anti-inflammatory Potential of Polyol-Synthesized Silver Nanoparticles. ACS omega. 2024;9(11):13208-13216.
[20] Khor S-H, Lee ML-Y, Basirun WJ, Juan J-C, Phang S-W. The effect of morphology of polyaniline on photodegradation of reactive black 5 dyes. Polymer Bulletin. 2024;81(8):7295-7327.
[21] Jayanti PD, Kusumah HP, Mahardhika LJ, Riswan M, Wahyuni S, Adrianto N, et al. Localized surface plasmon resonance properties of green synthesized Ag/rGO composite nanoparticles utilizing Amaranthus viridis extract for biosensor applications. Journal of Science: Advanced Materials and Devices. 2024;9(3):100747.
[22] Modak P, Tayade N, Itankar S, Mahant Y, editors. Synthesis, optical study and band gap energy of polyaniline/graphene nanocomposite. AIP Conference Proceedings; AIP Publishing. 2024.
[23] Kumar D, Sharma S, Khare N. Enhanced photoelectrochemical performance of plasmonic Ag nanoparticles grafted ternary Ag/PaNi/NaNbO3 nanocomposite photoanode for photoelectrochemical water splitting. Renewable Energy. 2020;156:173-182.
[24] Moosavy M-H, de la Guardia M, Mokhtarzadeh A, Khatibi SA, Hosseinzadeh N, Hajipour N. Green synthesis, characterization, and biological evaluation of gold and silver nanoparticles using Mentha spicata essential oil. Scientific Reports. 2023;13(1):7230.
[25] Turkten N, Karatas Y, Uyguner-Demirel CS, Bekbolet M. Preparation of PANI modified TiO2 and characterization under pre-and post-photocatalytic conditions. Environmental Science and Pollution Research. 2023;30(51):111182-111207.

[26] Al-Mahmud MR, Shishir MKH, Ahmed S, Tabassum S, Sadia SI, Sachchu MMH, et al. Stoichiometry crystallographic phase analysis and crystallinity integration of silver nanoparticles: A Rietveld refinement study. Journal of Crystal Growth. 2024;643:127815.
[27] Badi N, Roy AS, Al-Aoh HA, Motawea MS, Alghamdi SA, M. Alsharari A, et al. Enhanced and Proficient Soft Template Array of Polyaniline—TiO2 Nanocomposites Fibers Prepared Using Anionic Surfactant for Fuel Cell Hydrogen Storage. Polymers. 2023;15(20):4186.
[28] Zaman Y, Ishaque MZ, Ajmal S, Shahzad M, Siddique AB, Hameed MU, et al. Tamed synthesis of AgNPs for photodegradation and anti-bacterial activity: effect of size and morphology. Inorganic Chemistry Communications. 2023;150:110523.
[29] Ali MH, Azad MAK, Khan K, Rahman MO, Chakma U, Kumer A. Analysis of crystallographic structures and properties of silver nanoparticles synthesized using PKL extract and nanoscale characterization techniques. ACS omega. 2023;8(31):28133-28142.
[30] Kroutil J, Laposa A, Povolny V, Klimsa L, Husak M. Gas sensor with different morphology of pani layer. Sensors. 2023;23(3):1106.
[31] Gautam SK, Panda S. Highly sensitive Cu-ethylenediamine/PANI composite sensor for NH3 detection at room temperature. Talanta. 2023;258:124418.
[32] Al-Mur BA, Ansari MO. Silver Anchored Polyaniline@ Molybdenum Disulfide Nanocomposite (Ag/Pani@ MoS2) for Highly Efficient Ammonia and Methanol Sensing under Ambient Conditions: A Mechanistic Approach. Nanomaterials. 2023;13(5):828.
[33] Muhammad Y, Shah M, Safi MA, Khattak SG, Aziz A, Hassan H. Highly selective and sensitive humidity sensor using reduced graphene oxide based iron oxide nanocomposites. Materials Science and Engineering: B. 2024;303:117324.
[34] Safi MA, Shah M. Study the effect of ZnO additive in rGO/ZnO nanocomposites for the investigation of ammonia sensing characteristics. Materials Science and Engineering: B. 2024;299:116999.
[35] Guan Y, Wang C, Yu H, Zou Z, Zhou Y, Cao G, Yao J. Flexible ZnO/PANI/nonwoven nanocomposite based high-sensitive NH3 gas sensor via vapor phase polymerization method. Materials Science for Energy Technologies. 2020;3:862-867.
[36] Hu Q, Wang Z, Chang J, Wan P, Huang J, Feng L. Design and preparation of hollow NiO sphere-polyaniline composite for NH3 gas sensing at room temperature. Sensors and Actuators B: Chemical. 2021;344:130179.
[37] Zheng Q-Y, Yang M, Dong X, Zhang X-F, Cheng X-L, Huo L-H, et al. ZnO/PANI nanoflake arrays sensor for ultra-low concentration and rapid detection of NO2 at room temperature. Rare Metals. 2023;42(2):536-544.
[38] Sonwane ND, Maity MD, Kondawar SB. Conducting polyaniline/SnO2 nanocomposite for room temperature hydrogen gas sensing. Materials Today: Proceedings. 2019;15:447-453.
[39] Karmakar N, Jain S, Fernandes R, Shah A, Patil U, Shimpi N, Kothari D. Enhanced Sensing Performance of an Ammonia Gas Sensor Based on Ag-Decorated ZnO Nanorods / Polyaniline Nanocomposite. ChemistrySelect. 2023;8(18):e202204284.
[40] Amu-Darko JNO, Hussain S, Gong Q, Zhang X, Xu Z, Wang M, et al. Highly sensitive In2O3/PANI nanosheets gas sensor for NO2 detection. Journal of Environmental Chemical Engineering. 2023;11(1):109211.
[41] Zhang B, Shang F, Shi X, Yao R, Wei F, Hou X, et al. Polyaniline/CuO Nanoparticle Composites for Use in Selective H2S Sensors. ACS Applied Nano Materials. 2023;6(19):18413-18425.